Geomechanics and Engineering, *Vol. 32, No. 3 (2023)255-270*
https://doi.org/10.12989/gae.2023.32.3.255

Three-dimensional numerical analysis of nonlinear phenomena of the tensile resistance of suction caissons

Azam Arefi[1a], Pooria Ahad[1b], Mehdi Bayat[2,3c] and Mohammad Silani*[1]

[1]*Department of Mechanical Engineering, Isfahan University of Technology, Isfahan, 84156-83111, Iran*
[2]*Department of Civil Engineering, Aalborg University, Aalborg, Denmark*
[3]*Current address: Svanehøj Danmark A/S, Fabriksparken 6, 9230 Svenstrup J, Denmark*

(*Received September 4, 2021, Revised December 30, 2022, Accepted January 13, 2023*)

Abstract. One of the main parameters that affect the design of suction caisson-supported offshore structures is uplift behavior. Pull-out of suction caissons is profoundly utilized as the offshore wind turbine foundations accompany by a tensile resistance that is a function of a complex interaction between the caisson dimensions, geometry, wall roughness, soil type, load history, pull-out rate, and many other parameters. In this paper, a parametric study using a 3-D finite element model (FEM) of a single offshore suction caisson (SOSC) surrounded by saturated soil is performed to examine the effect of some key factors on the tensile resistance of the suction bucket foundation. Among the aforementioned parameters, caisson geometry and uplift loading as well as the difference between the tensile resistance and suction pressure on the behavior of the soil-foundation system including tensile capacity are investigated. For this purpose, a full model including 3-D suction caisson, soil, and soil-structure interaction (SSI) is developed in Abaqus based on the $u-p$ formulation accounting for soil displacement (u) and pore pressure, P.The dynamic responses of foundations are compared and validated with the known results from the literature. The paper has focused on the effect of geometry change of 3-D SOSC to present the soil-structure interaction and the tensile capacity. Different 3-D caisson models such as triangular, pentagonal, hexagonal, and octagonal are employed. It is observed that regardless of the caisson geometry, by increasing the uplift loading rate, the tensile resistance increases. More specifically, it is found that the resistance to pull-out of the cylinder is higher than the other geometries and this geometry is the optimum one for designing caissons.

Keywords: 3-D finite element analysis; suction caisson; tensile capacity; $u-p$ formulation

1. Introduction

Limited access to the energy resources such as oil, gas, and coal along with environmental pollution produced during their exploitation, recently, the development of renewable energy sources gained a lot of attention. Among various energy resources such as wind, sun, and waves, wind energy is the most rapidly developing one (Schwägerl 2016). Despite the high-energy density and lower turbulence of offshore wind power (Oh *et al.* 2018), the construction costs of offshore wind frames are greater than that of onshore ones (Musial *et al.* 2010). Therefore, selecting a suitable offshore wind energy converter foundation type and its optimal design are the most important factors contributing to lowering the cost. Among various types of foundations including gravity-based, monopile, and suction caisson, the suction caisson type is the most promising due to small installation vibration and noise (Breton and Moe 2009). Moreover, the steel weight of this foundation is less than half compared to the traditional monopile foundations (Ibsen *et al.* 2005, Gonzalez 2017). Monopods and multi-pods are two typical types of these structures constructed of an open-ended base (skirt) and a closed top (lid) in which the ratio of the caisson diameter to the skirt length ranges from 0.25 to 12 (Villalobos 2006, Larsen 2008, Roa *et al.* 1997, Iskander *et al.* 2002, Achmus *et al.* 2014). Caissons with an embedment ratio of 2 or higher are typically used for clayey soils while caissons with lower embedment ratios are appropriate for sandy soil conditions (Houlsby *et al.* 2005, Cotter 2009). The dominant loads for suction caissons when used as anchors for tension leg platforms or as foundations on a jacket structure are axial (Nielsen 2019). For relatively light structures such as wind turbines, the overturning moment resulting from large aerodynamic loads can lead to tensile loading and pull out of the individual foundations of the structure. Consequently, the tensile resistance of these foundations is a key factor for determining their service life and should be accounted for in foundation design.

Suction caissons were first developed for floating platforms in the gas and oil industry (Zhu *et al.* 2011). The application of these foundations for offshore wind turbines encouraged a lot of researchers (Senders 2008, Alavi *et al.* 2010, Fattah *et al.* 2013, Thieken *et al.* 2014, Vaitkunaite *et*

*Corresponding author, Associate Professor
E-mail: silani@iut.ac.ir
[a]Ph.D.
E-mail: azam_arefy@yahoo.com
[b]M.Sc.
E-mail: pooria.ahad@gmail.com
[c]Ph.D.
E-mail: bayat.me@gmail.com

ISSN: 2005-307X (Print), 2092-6219 (Online)

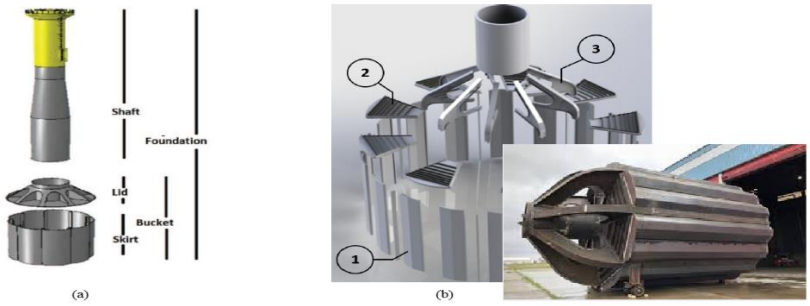

Fig. 1 Bucket geometries (a) (Schløer *et al.* 2016) and (b) (Gonzalez 2017).

al. 2014, Kim *et al.* 2017, Chong *et al.* 2019, Nielsen 2019, Hendriyawan 2019, Ahlinhan 2020) to investigate their tensile resistance. Achmus and Thieken (2014) conducted numerical simulations based on the combination of pore fluid diffusion and stress analysis. They investigated the effects of loading rate, soil permeability, and pore fluid displacement on the bucket load-bearing capacity. They announced that the effects of dynamics components resulting from pore fluid displacement are not considered and can be ignored. Sorensen *et al.* (2017) examined the tensile resistance of suction buckets based on 3 different numerical formulations. There was a good match between various results. Since inertia effects are negligible for most of the pull-out velocities, they concluded that available formulations in commercial software are appropriate for the analysis of the tensile resistance of suction buckets. Ahmed and Hawlader (2014) performed 3-D analyses of monopod suction caissons subjected to various oblique loadings. The effects of loading angle, mooring position, and aspect ratio on pullout capacity and rotation of the caisson were examined. Bagheri and Kim (2019) evaluated the mechanical behavior of caissons with different dimensions embedded in soils with different densities subjected to monotonic and cyclic loadings by conducting a 3-D finite element model of the foundation and the seabed. The results indicated that the foundation response is more sensitive to the soil density in comparison with its geometry. Ma *et al.* (2019) studied the shallow bucket foundation response to lateral loadings. Analysis of the Load-Displacement relation along with pore pressure and soil pressure revealed the foundation deformation pattern and also it was observed that the accumulation of pore pressure leads to a decreasing the anti-overturning bearing capacity of the foundation. Skau *et al.* (2019) provided a methodology through which the effect of caisson flexibility can be incorporated in finite element modeling by the definition of a macro element. Their results confirmed that caisson flexibility influences the coupling between moment and horizontal load. It also affects the foundation stiffness felt by the other structures attached to it. Jin *et al.* (2019) performed various 3-D numerical analyses of caisson foundations in the sand by applying complex combined loadings to the caisson to identify the failure envelope in various spaces. Latini and Zania (2019) examined the dynamic stiffness and damping coefficients of suction caissons embedded in a viscoelastic soil layer over bedrock under vertical dynamic load. It was observed that soil stiffness variation with depth and skirt length affects the dynamic response dramatically.

To investigate the soil deformations and installation mechanism of giant circular open caissons in undrained clay, Lai *et al.* (2020) modeled the process using 3-D simulations by employing Coupled Eulerian-Lagrangian approach. The plastic zone, deformed soil flow, stress distribution, and penetration resistance developed in clay were effectively captured to investigate the installation mechanism. Faizi *et al.* (2019) proposed a new hybrid tripod bucket foundation able to resist overturning moments considerably in comparison with the conventional tripod types. The load-bearing capacity of composite bucket foundations with and without compartment plates installed in layered soil was investigated by Ding *et al.* (2020) under combined loadings. They showed that Compartments improve the integrity of the bucket foundation and change the dominant load-bearing mode.

Bucking of the cylindrical buckets and other installation problems motivated researchers to investigate geometries other than cylindrical ones (Schløer *et al.* 2016, Gonzalez 2017). In this research, multi-shell foundations reinforced with stiffeners were investigated (Fig. 1).

Although a wide range of research has been devoted to the study of the mechanical behavior of suction caisson foundations, most of them are focused on examining the effects of variation of bucket dimension, pull-out rate, loading, and soil permeability on its mechanical response, especially on the tensile resistance. It is to be mentioned that Buckets with non-circular geometries can solve some installation issues. Therefore, investigating the effect of geometry change is substantial for an optimized design of these structures and obtaining their ultimate tensile resistance, too. To the best of the authors' information, there has not been reported such incremental parametric study of SOSC offshore wind turbine foundation considering geometry change in 3-D space. In the present work, FEM with a nonlinear material model and transient analysis has been developed to perform a 3-D numerical analysis of nonlinear phenomena of the SOSC tensile resistance. Comprehensive numerical analyses have been performed to investigate the effect of bucket geometry. The soil material model has been developed as a user material model (UMAT) in Abaqus and a computer set was performed to present the results for the 3-D model in the time domain. Furthermore, the effects of geometry change and pull-out rate on the tensile resistance and the difference between tensile resistance and suction pressure on an MSC have

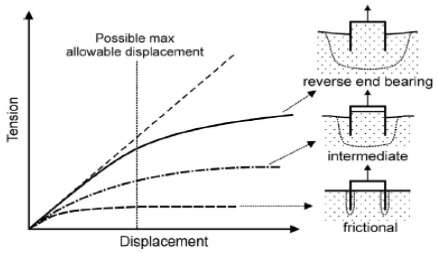

Fig. 2 Force-displacement curves and corresponding failure mechanisms for suction caissons under tensile loading (Senders 2008)

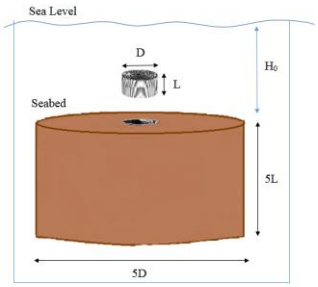

Fig. 3 A schematic view of the seabed and a suction bucket foundation

been analyzed. The experimental results of cone penetration tests and drained triaxial tests at Aalborg University (Ibsen *et al.* 2009) were utilized for material calibration.

Following this introduction, Section 2 presents the effective parameters on vertical resistance of SOSCs in offshore wind turbines and Section 3 contains the governing coupled *u-p* equations of the saturated soil. In Section 4, the model, mechanical properties and calibration, boundary and loading conditions, and contact constraints are described. In Section 5, the numerical solution is validated by comparison to the available results. The tensile resistance, suction pressure, and also the difference between these parameters are discussed and described for different geometries in Section 6. Some concluding remarks are presented in Section 7.

2. Effective parameters on the suction caisson tensile resistance

Drainage conditions classified as fully-drained, partially-drained, and undrained conditions determine the load-bearing capacity of a suction caisson under tensile loading after installation. These conditions depend on the soil permeability, loading rate, and bucket dimensions.

In fully-drained conditions, the bucket weight and the friction on the inner and outer perimeter of the skirt control the bucket tensile resistance. In this case, a gap is formed between the bucket lid and the soil surface. For undrained conditions, due to the lack of gap formation arising from suction pressure, the whole soil inside the bucket moves upward and shear forces distribute on the soil surrounding the bucket outside the perimeter. In this case, frictional forces have a great contribution to the bucket tensile resistance, and the bucket resistance is higher than that in the fully-drained conditions. The bucket tensile behavior for partially-drained conditions locates between these two extreme scenarios. Fig. 2 illustrates these conditions briefly.

3. The u-p formulation

Among various formulations for modeling saturated soil behaviors (Zienkiewicz and Shiomi 1984), $u-p-U$ the formulation in which the displacement of the soil skeleton, the pore fluid pressure, and the pore fluid displacement play a significant role is the most widely used. Since for slow phenomena, the fluid acceleration accompanies insignificant inertia forces, in numerous FE software, *u-p* the formulation is adopted in which only the soil skeleton movement and the pore fluid pressure are considered.

Combination of equilibrium conditions for each phase in saturated soil, the continuity equation of the fluid flow, and also a proper constitutive relation results in the formation of the *u-p* formulation. The equilibrium condition for the soil skeleton in the *u-p* formulation is governed by (Sørensen *et al.* 2017)

$$(k(-p_{,i}-\rho_f\ddot{u}+\rho_f b_i))_{,i}+\alpha\dot{\varepsilon}_{ll}+\frac{1}{Q}\dot{p}=0 \tag{1}$$

where, p, being the pore pressure and $\ddot{u}_l$ is the acceleration of the solid phase. k denotes the soil skeleton permeability which depends on the hydraulic conductivity. b_i,ε, and ρ_f are the body force, strain tensor, and fluid viscosity, respectively. α is the Biot coefficient defined by

$$\alpha=1-\frac{K}{K_s} \tag{2}$$

K and K_s are the bulk modulus of the soil skeleton and the average bulk modulus of the soil skeleton constituents, respectively.

In Eq. (1), the combined storage capacity of the solid and fluid results from a pressure change is shown by $\frac{1}{Q}$ which is given by

$$\frac{1}{Q}=\frac{n}{K_f}+\frac{\alpha-n}{K_s} \tag{3}$$

where K_f is the fluid bulk modulus and n is the porosity.

4. Finite element modeling

This section details various aspects of modeling pull-out tests. The FE analyses were performed using finite element software Abaqus 6.14. In Fig. 3, a schematic view of the model in which Baskarp sand no. 15 is assumed to constitute the seabed, is visualized. Variation of tensile resistance with different pull-out rates from 1e-6 m/s corresponding to the soil drained behavior to 0.1m/s in steps of one order of magnitude is investigated.

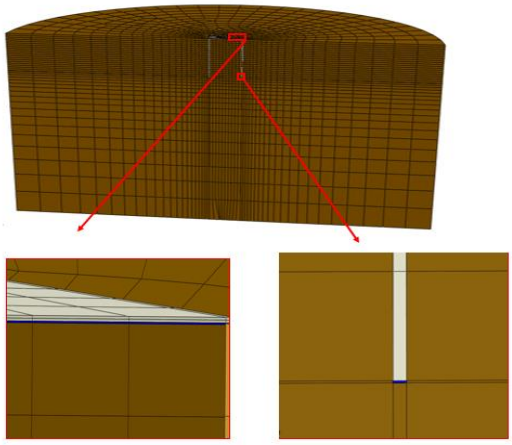

Fig. 4 Close-up view of water elements under (a) bucket lid and (b) bucket skirt

4.1 Modeling of the SOSC and surrounding soil

A cylindrical bucket with a skirt length of L=10 m, an inner diameter of D=10 m, and a thickness of t=30 mm embedded in the seabed, and a cylinder with an outer diameter of 50 m and height of 50 m, was modeled. These dimensions were assigned to the seabed to avoid boundary effects on the results. For modeling the bucket domain, ordinary continuum material, and for the soil a porous material model was used. Taking the advantage of geometry and loading symmetry, only a quarter of the SOSC foundation and the surrounding soil was simulated. On account of the possible formation of the water-filled gap beneath the bucket lid and skirt, a soft layer with a thickness of 10 mm was integrated into the model (Thieken *et al.* 2014, Achmus and Thieken 2014, Cao *et al.* 2002).

4.1.1 Material models and discretization

The steel SOSC is modeled as a linear elastic material with Young's Modulus 210GPa, Poisson's ratio of 0.25, and a density of 7500 Kg/m^3 (Sørensen *et al.* 2017). It is assumed that Baskarp sand no. 15 with void ratio 0.59 and bulk modulus 36.4GPa (Skempton 1961) constitutes the solid phase of the seabed soil fully saturated with water in which water density and bulk modulus are equal to 1000 Kg/m^3 and 2.05 GPa, respectively. On account of the dilative and plastic behavior of the soil solid phase, the Pressure-dependent Mohr-coulomb model is employed. For material calibration, the experimental results of cone penetration tests and drained triaxial tests at Aalborg University (Ibsen *et al.* 2009) were utilized. Table. 1 summarizes other soil solid phase parameters (Sørensen *et al.* 2017, Sørensen 2016). It is to be mentioned that the larger the soil permeability is, the smaller the suction pressure and total resistance will be (Achmus *et al.* 2014). Therefore, for larger permeabilities, the behavior becomes more similar to the smaller pull-out rates. In the present manuscript various pull-out rates are investigated and to make the simulations more cost-effective, the initial permeability of the soil is used for the simulations. It should be noted that a sensitivity analysis and uncertainty propagation could be very helpful to investigate the influence of all uncertain input parameters (Samaniego *et al.* 2020).

Table 1 Properties of the soil solid phase (Sørensen *et al.* 2017, Sørensen 2016)

Description	Parameter	Value
Solid Phase Density	ρ_s	2.644e3 Kg/m3
Porosity	n	0.373
permeability	k	6.77e-9 m3s/Kg
Hydraulic conductivity	k_D	6.65e-5 m/s
Coefficient of earth pressure at rest	K_0	0.33

Considering the negligible permeability of steel, C3D8R elements with no pressure degree of freedom were used to discretize the bucket. The *u-p* formulation was employed to model the soil domain as a porous material. Since this constitutive model doesn't exist in Abaqus, a user material subroutine (UMAT) was implemented in Intel Fortran which is linked by Abaqus using Visual Studio. To mesh the soil, C3D8P elements with displacement and pressure degrees of freedom accounting for porosity and pore pressure due to fluid flow into the soil were applied. C3D8PH elements able to account for pressure degree of freedom and incompressible material behavior with a very low Young's modulus and poison's ratio of 0.499 were generated beneath the bucket lid and skirt to simulate the water behavior. These elements were located to simulate seepage into the gap formed beneath the lid inside the bucket. It should be noted that to prevent convergence problems, only one row of water elements should be applied (Fig. 4).

In C3D8PH elements, pressure is considered an extra unknown. These elements are applied when the material is incompressible ($\vartheta = 0.5$). Since the pressure in these elements is unknown, simple elements cannot be used for the simulation of incompressible behavior. By simulation of one element with incompressible material behavior under hydrostatic loading, the volume of the element will not

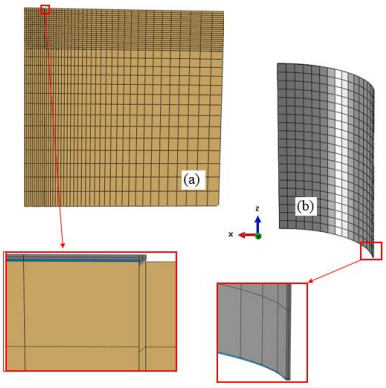

Fig. 5 Modeling strategy: (a) the surrounding soil, bucket lid, and the water beneath it, and (b) the bucket skirt and the water beneath it are modeled as two separate parts

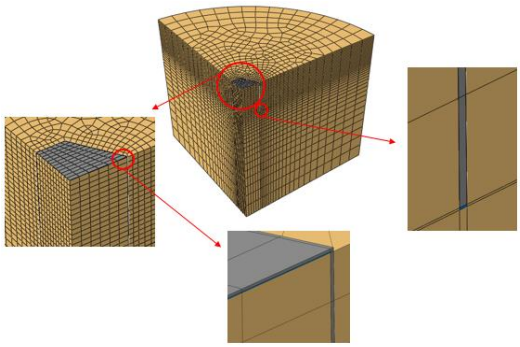

Fig. 6 A schematic view of the model and its details

change. Furthermore, compressive stresses cannot be computed using displacements of the nodes. Consequently, hybrid elements with an extra degree of freedom for the calculation of compressive stresses can solve this problem.

It should be noted that all parts except the bucket skirt are modeled as a whole to eliminate the application of redundant constraints. Therefore, different parts are distinguished by the definition of different sections and by assigning special material models and elements. More details are provided in Fig. 5.

The model is discretized such that the nodes along the common boundaries place identically to apply node-to-node contact constraint implemented using the Lagrange multiplier method (Wriggers and Laursen 2006). Fig. 6 shows a schematic of the model and its discretization.

4.1.2 Boundary conditions and constraints

Radial displacement of the soil's outer and inner boundaries i.e., r=50 m and 0 mm, is constrained along the cylinder height. Soil vertical displacement at the bottom (z=-50 m) is also set equal to zero. Symmetric constraints are applied on the symmetry planes e.g., symmetric constraint on the Y-Z plane is defined as ($u_x = \theta_y = \theta_z = 0$) in which u_x, θ_y, θ_z are displacement in X direction and rotation in Y and Z directions, respectively. Fig. 7 shows applied boundary conditions.

One of the limitations of this modeling strategy is that its simulation results are only valid for water in the liquid

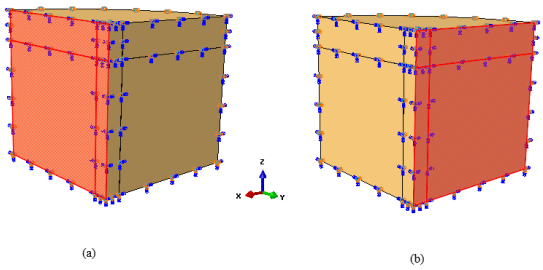

Fig. 7 Applied symmetric boundary conditions on (a) x plane and (b) Y plane

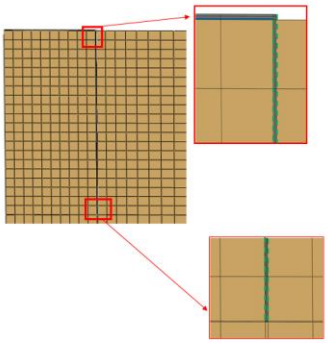

Fig. 8 A schematic view of the boundaries on which frictional interaction between the soil skeleton and the bucket is defined

phase. As soon as a phase change occurs (liquid to gas), due to the formation of porosities, the results are not valid anymore. When pore pressure is less than the cavitation pressure, a phase change occurs and dramatically affects liquid properties and its ability in flowing through the soil which leads to the variation of bucket tensile resistance. In consequence, the results are valid for pressures higher than the cavitation pressure (p_c= -100 Kpa). In the absence of cavitation, the pore pressure effect on the bucket resistance is related to the pore pressure gradient and also the relative pressure difference between the inside and outside of the bucket. Therefore, the pore pressure is measured concerning the hydrostatic pressure at the seabed ($\rho g H_0$) which H_0 denotes the water depth. Based on this approach, as long as Eq. (4) is governed, the results are valid.

$$p + p_0 > p_c \tag{4}$$

The pore pressure for the seabed, outside the bucket, is assumed to be equal to zero to allow fluid flow across the boundary. Moreover, to allow water to flow into the soil along the outer radial boundary and at the bottom, the hydrostatic pressure, $p=\rho_f g z$ is set as the pore pressure in these regions.

Contact constraints are applied along the vertical boundary formed between the bucket and the soil (Fig. 8). This constraint is implemented by the node-to-node contact elements implemented using the Lagrangian multiplier method. Between these surfaces, Frictional slip-stick formulation is governed by which frictional capacity, τ_f, is defined as

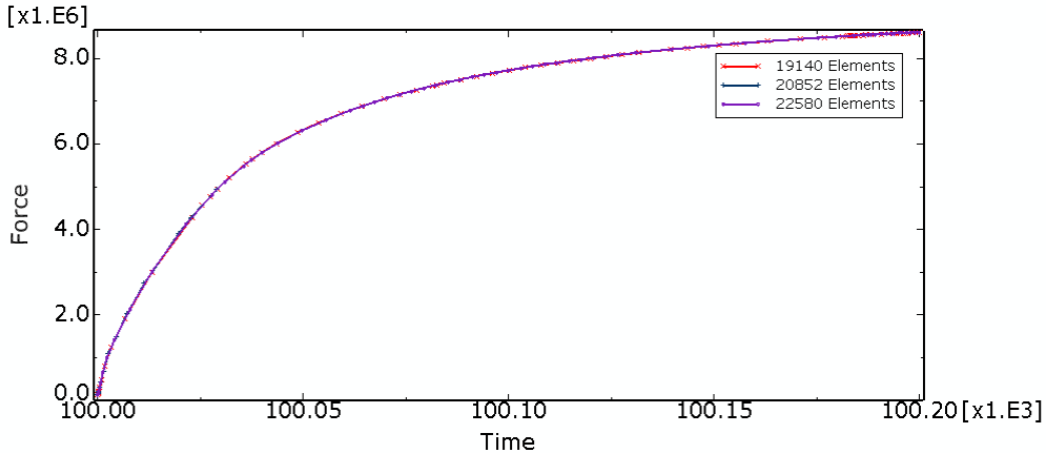

Fig. 9 Results of convergence analysis utilizing resistance force for cylindrical buckets

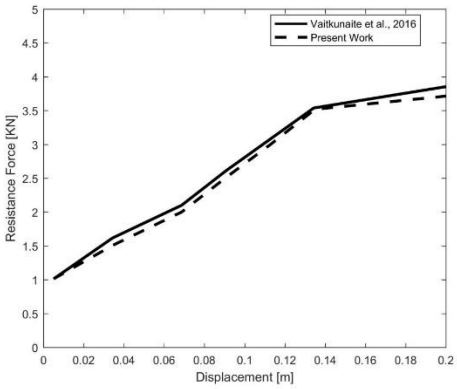

Fig. 10 Comparison of the total resistance with the results of Vaitkunaite *et al.* (2016) for the velocity of 1e-3 m/s

$$\left|\tau_f\right| \le \sigma_n' \tan(\delta) + a \tag{5}$$

Where σ_n, δ, and a are effective normal stress, friction angle, and cohesion, respectively. In the present work, δ=26° and a= 0 Kpa are considered (Sørensen *et al.* 2017).

Owing to the continuity of the soil skeleton, bucket lid, and the water beneath it (Fig. 5), only the common surface between the top surface of the bucket skirt and lid and also the lower surface of the water beneath the bucket skirt is restricted by applying tie constraint.

4.1.3 Initial and loading conditions

To define the initial condition and apply the load, it is assumed that at the beginning of the simulation ($t = t_0$) the bucket has been installed and the soil stress distribution is characterized by the geostatic conditions under hydrostatic pressure. Therefore, the initial pore pressure variation is defined as

$$p(t_0) = \rho_f gz \tag{6}$$

Since the installation process is not taken into account, the simulation started when the upward external force adjusted the bucket weight. To model these forces, a constant vertical displacement rate on the nodes at the top of the bucket lid (according to Eq. (7)) displaces the bucket upward. The gravity force is also applied to the whole model accounting for the weight effect. In geostatic problems, the initial conditions should be defined in such a way that the solution starts after equilibrium. Consequently, initial stresses and displacements accompanied by the bucket installation are equilibrated defining a geostatic step at the beginning of the solution. Then, the bucket is pulled out slowly by 2 ms. Since the effects of pore pressure on the soil are followed, the transient *SOILS analysis was selected as the analysis procedure. In the final step, a heave of the bucket lid with constant velocity leads to the applying tensile loads on the bucket. For this step, again * SOILS analysis was employed and the time step is set such that the bucket is raised 200 mm.

$$p(t_0) = \rho_f gz \tag{7}$$

4.1.4 Mesh convergence analysis

To study the effect of element sizes on the results, meshes with different numbers of elements were generated for the buckets with cylindrical shapes. In Fig. 9, the variation of the resistance force during pull-out loading at

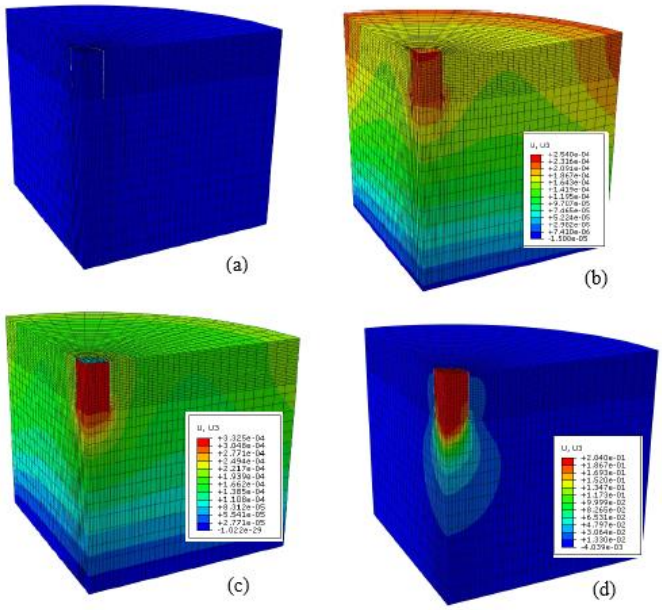

Fig. 11 Vertical displacement contours for the velocity of 0.1 m/s. (a) beginning of the solution, (b) geostatic solution, (c) initial pull-out and (d) tension with constant velocity

the velocity of 1e-3 m/s is plotted considering the various elements. It can be seen that coarse models with a smaller number of elements can approximately provide the same results as the models with finer meshes. In the trade-off between accuracy and simulation costs, the best number of elements were used to simulate various geometries.

5. Validation

For validation, the results of the FE model of a caisson are compared against the observations of an approximately 1:20 scale model pull-out test conducted by Vaitkunaite *et al.* (2016). The simulated 3-D caisson undergoing tension loading at the velocity of 1e-3 m/s has a skirt length of 250 mm, lid diameter of 500 mm, and thickness of 6 mm. besides, the soil base was chosen to have a depth and a radius of 1500 mm. The simulation procedure explained insection 4 was used to extract the FEM results. Fig. 11 presents the results of the model test performed by Vaitkunaite *et al.* (2016) and that of FEM. The comparison suggests that the FE model could predict tensile behavior appropriately.

6. Results and discussion

6.1 Cylindrical geometry

This section summarizes finite element results of 3-D cylindrical SOSC. Bucket resistance vs. vertical displacement for various velocities is presented. Since suction pressure is one of the most important components that affect the bucket tensile resistance, variation of suction pressure concerning the vertical displacement is also reported.

Contours of the suction bucket vertical displacement for the pull-out rate of 0.1 m/s at the end of each step i.e., a) initial step, b) geostatic solution, c) initial tension, and d) tension with a constant velocity until reaching a heave of 200 mm are given in Fig. 11.

It can be seen that although there is not any loading in the geostatic solution step, the soil saturation and water seepage lead to the soil heave. Consequently, some displacement can be observed. In addition, the bucket weight causes its downward movement and prevents soil uplift in the zone surrounding the bucket.

Fig. 12 displays the gap expansion beneath the bucket lid for three different pull-out rates. The difference in the behavior arises from velocity difference corresponding to drained (low velocities), partially-drained (mean velocities), and undrained (high velocity) conditions, as was reported by Senders (2008). In drained conditions, sufficient seepage is possible and suction pressure will not occur. As a result, the water elements expand completely and the soil will not displace vertically. For high displacement rates, suction pressure hinders gap expansion (Fig. 12, top). For the pull-out rate of 1e-2 m/s, gap expansion is less than the bucket displacement. In such partially-drained soils, the more the pull-out rate is, the less the gap will expand.

Fig. 13 shows the resistance forces vs. bucket vertical displacement for various loading rates. In these figures solid and dashed lines show the total resistance and suction pressure, respectively. The difference between these curves indicates the frictional forces between the soil and the skirt's internal and external surfaces. It can be seen that the bucket total resistance highly depends on the suction pressure such that by increasing the pull-out rate an undrained behavior is governed and the total resistance increases dramatically. As the pull-out rate decreases, drained behavior is more obvious and the suction pressure effect minimizes. Suction pressure for various velocities is visualized in Fig. 14 which

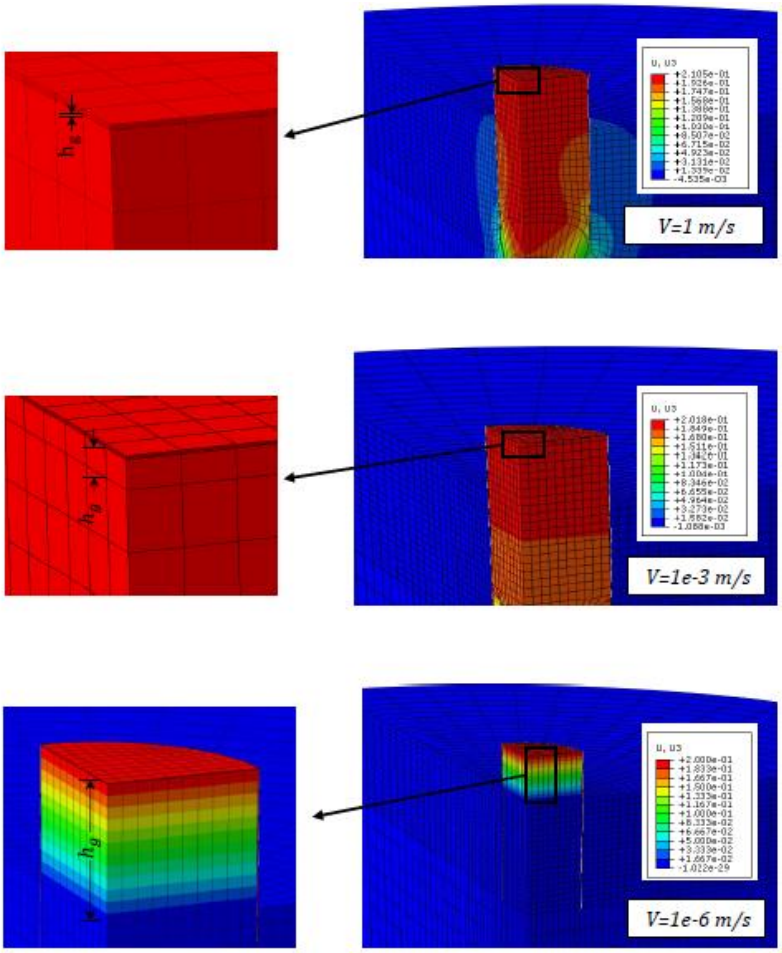

Fig. 12 Water elements expansion beneath the bucket lid corresponding to various velocities

clarifies this claim. In this case, the only factors that determine the bucket resistance are friction forces on the internal and external surfaces of the bucket skirt and a small contribution of the bucket weight. Besides, the more the velocity, the higher the ultimate resistance will be. It can be predicted that in higher velocities, the ultimate resistance will not reach even in very large displacements. It should be emphasized that various experimental tests conducted by Vaitkunaite *et al.* (2016) considering different pull-out rates confirm the trends and mechanical responses obtained with 3-D FEM results in the present work.

The development of the difference between the tensile resistance and suction pressure for various rates is presented in Fig. 15. By increasing the pull-out rate, the soil-drained behavior changes to the undrained one and as a result, the difference between tensile resistance and suction pressure decreases.

Figs. 16(a) and 16(b) show the ultimate tensile resistance and peak pressure for various velocities, respectively. As the extraction rate increases, the ultimate tensile resistance and peak pressure increase as well. In high velocities undrained behavior is governed; in this case, as explained in section 2, suction pressure develops under the lid and frictional forces have more contribution to the total resistance and the bucket resistance and suction pressure are higher than those in low velocities.

6.2 New geometries

After evaluating the simulation procedure, in this section, 3-D models with different geometries, inscribed and peripheral in a reference circle, such as a triangle, pentagon, hexagon, and octagon are studied. In Fig. 17, inscribed and peripheral triangles and hexagons are plotted.

Since triangular and pentagonal geometries only have one symmetry plane, half of the model is considered and for the other two, a quarter of the model is simulated. The methodology, boundary conditions, constraints, and material models are the same as the cylindrical one. For all geometries, bucket height and thickness are the same but due to the difference in their geometries, their volume and weight are different. The FE models of the triangle and hexagon are described in Fig. 18.

The variation of suction pressure and total resistance force concerning the displacement for some geometries is plotted in Figs. 19 and 20, respectively. In all of the figures, the graphs related to circular geometry are included as a reference solution. It can be seen that irrespective of the geometry, variation of resistance forces concerning the vertical displacements follow the same trends similar to that of the circular one for various velocities. The more the velocity increases, the more the resistance force will be. As

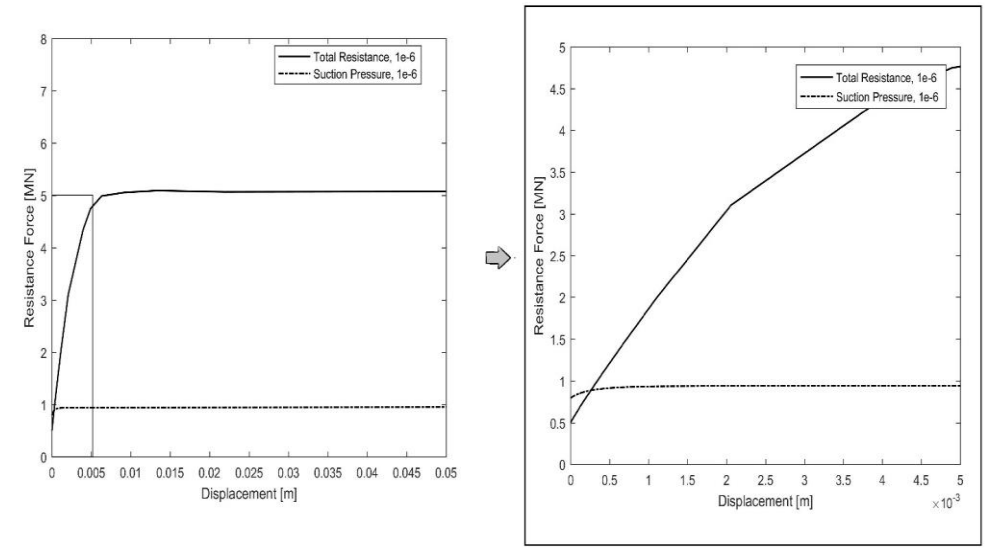

(a)

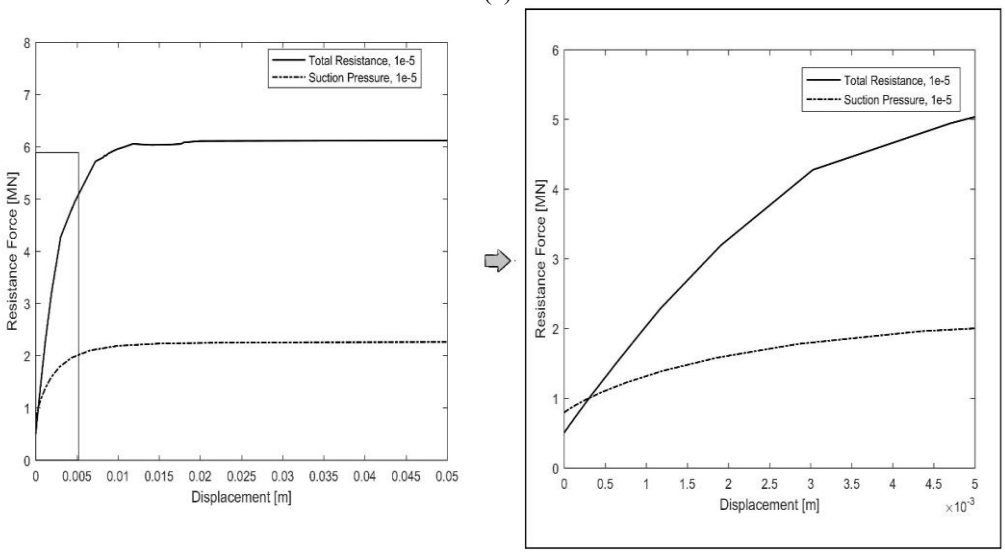

(b)

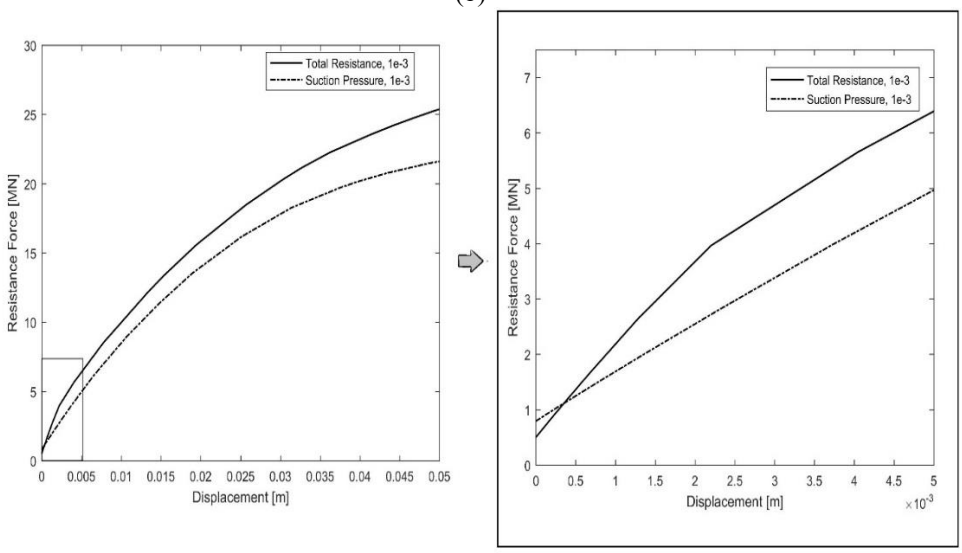

(c)

Fig. 13 Resistance forces for different velocities (a) 1e-6, (b) 1e-5, (c) 1e-4 and (d) 1e-3 m/s

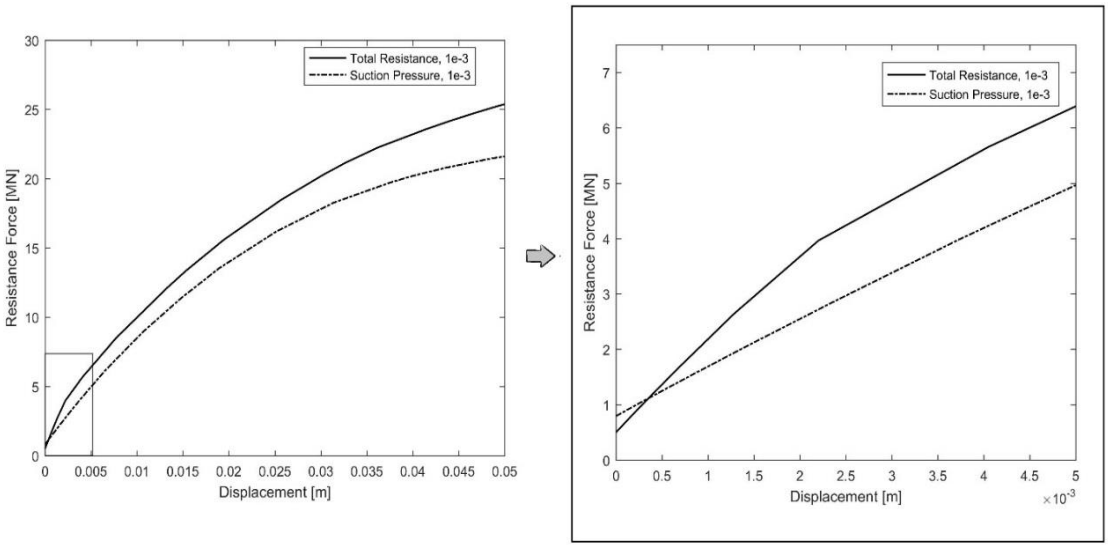

(d)

Fig. 13 Continued

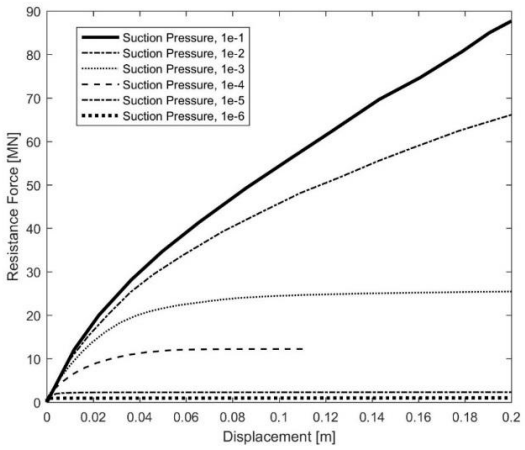

Fig. 14 Suction pressure versus displacement for various velocities

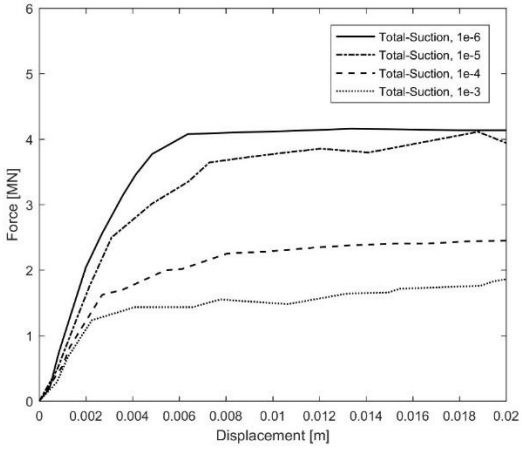

Fig. 15 Variation of the difference between total resistance and suction pressure with displacement for various velocities

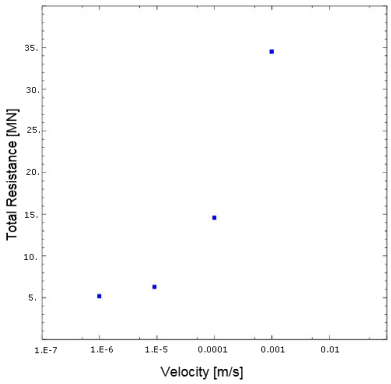

(a)

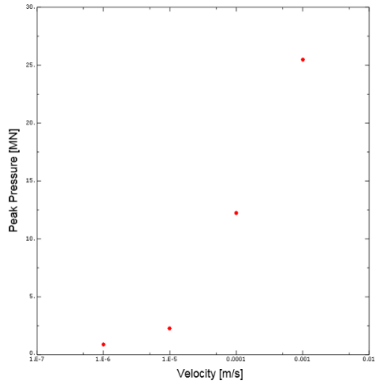

(b)

Fig. 16 (a) ultimate tensile resistance and (b) peak pressure for various velocities

the pull-out rate decreases, the resistance force decreases, too. In very low velocities, due to the decrease of suction pressure, the total resistance force is limited to the frictional resistance. The ultimate capacity of the bucket is reached at the displacement of 200 mm in lower velocities, whereas in higher velocities, the ultimate resistance will not reach. A

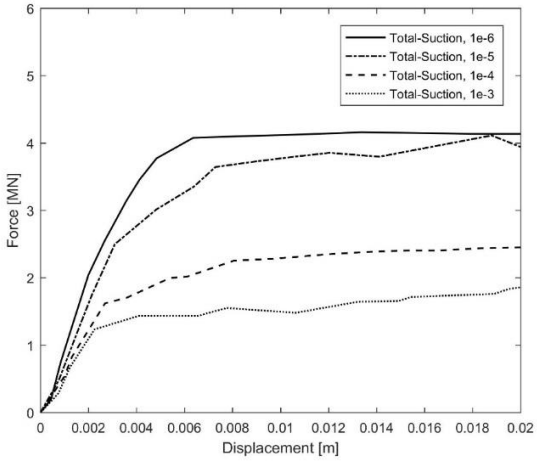

Fig. 17 Inscribed and peripheral (a) triangle and (b) hexagon in a reference circle

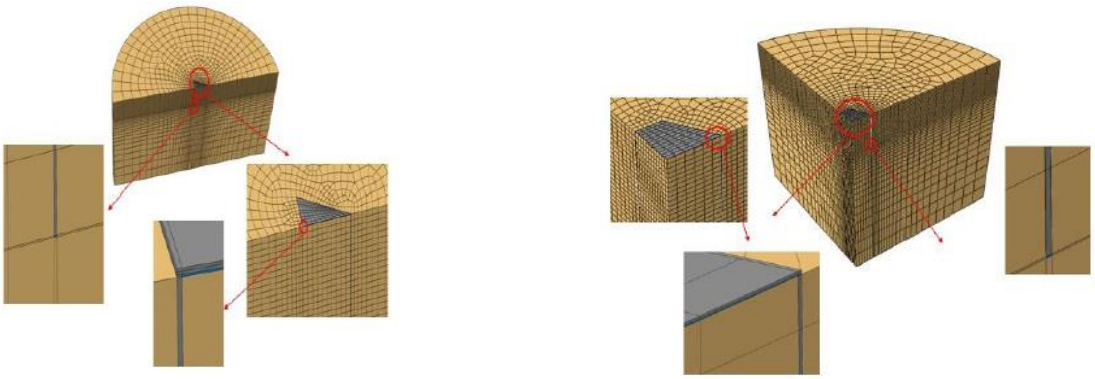

(a) (b)

Fig. 18 FE model of (a) triangular and (b) hexagonal suction caissons in the soil

close-up view of these figures shows that the effect of the loading rate on the initial resistance of the bucket is less than the ultimate resistance. As a consequence, considerable resistance is provided in very large displacements. In these figures, all curves start from a nonzero value denoting the resistance corresponding to the bucket weight.

Figs. 19 and 20 reveal that the more the geometry of the bucket is similar to the cylinder, the more the mechanical response of the bucket converges to that of the reference cylinder. This is more obvious for peripheral geometries. For instance, the total resistances in the 50 mm heave of the bucket for the peripheral octagon are 13 MPa and 6.2 MPa, at velocities of 1e-4 and 1e-5 m/s, respectively which is very close to those of the cylindrical geometry (14 MPa and 6 MPa).

It should be emphasized that for new geometries, FE results are reported for low velocities accounting for the effects of friction. Since in low velocities, frictional forces close-up view of these figures shows that the effect of the loading rate on the initial resistance of the bucket is less than the ultimate resistance. As a consequence, considerable resistance is provided in very large displacements. In these figures, all curves start from a nonzero value denoting the resistance corresponding to the bucket weight.

7. Conclusions

In this paper, three-dimensional FE analyses were employed to investigate one of the challenging topics related to suction caisson-supported offshore structures such as offshore platforms and wind turbines. Caisson resistance against uplift loading is very important in designing these structures that can be affected by caisson geometry. Furthermore, the bearing capacity and suction pressure of the SOSC foundations with various geometries such as triangle, pentagon, hexagon, and octagon in saturated soil were studied considering various loading rates. First, a 3-D model was developed to simulate the soil, bucket, and water accounting for the soil dilative and plastic behavior and also seepage and gap extension for cylindrical geometry as a reference solution. After verification of the reference model and mesh convergence analysis of the results, the results in the form of Total Resistance-Displacement and Suction-Displacement plots for all geometries were provided. It was concluded that regardless of the 3-D SOSC geometry, the more the velocity is, the more the tensile resistance will be. At high speeds, the development of suction pressure within the interior of the bucket in response to the pull-out determined the suction

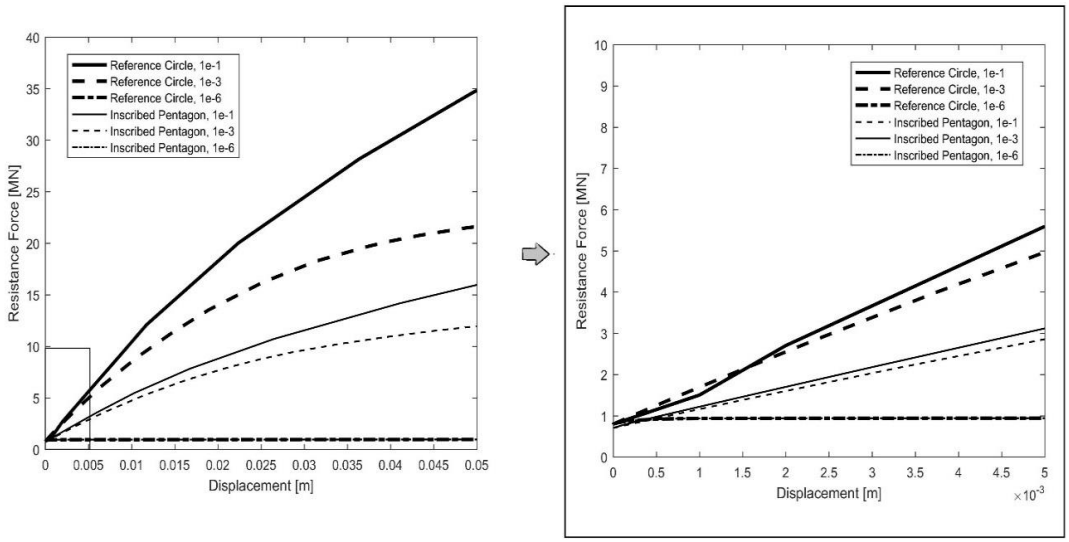

(a)

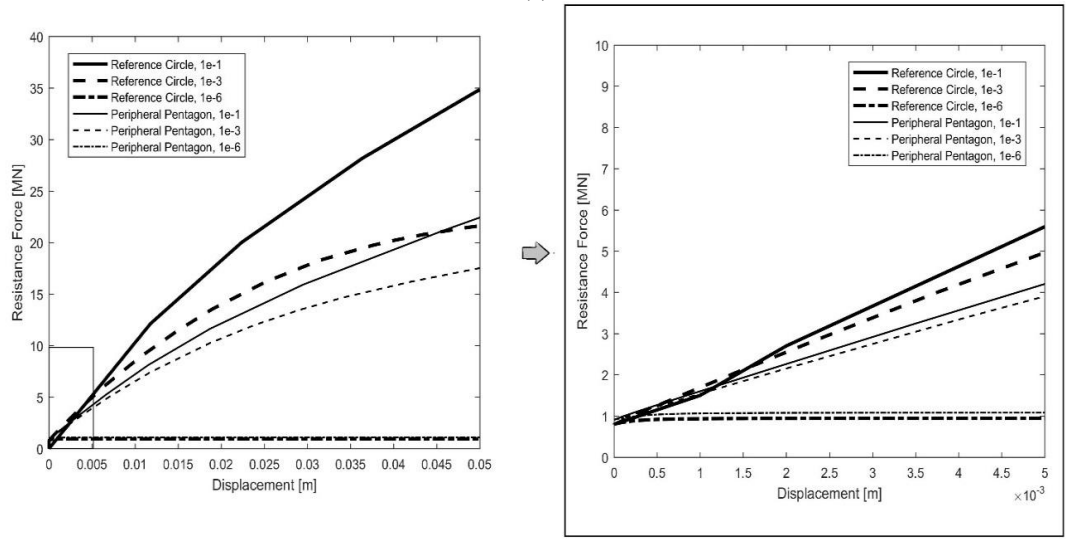

(b)

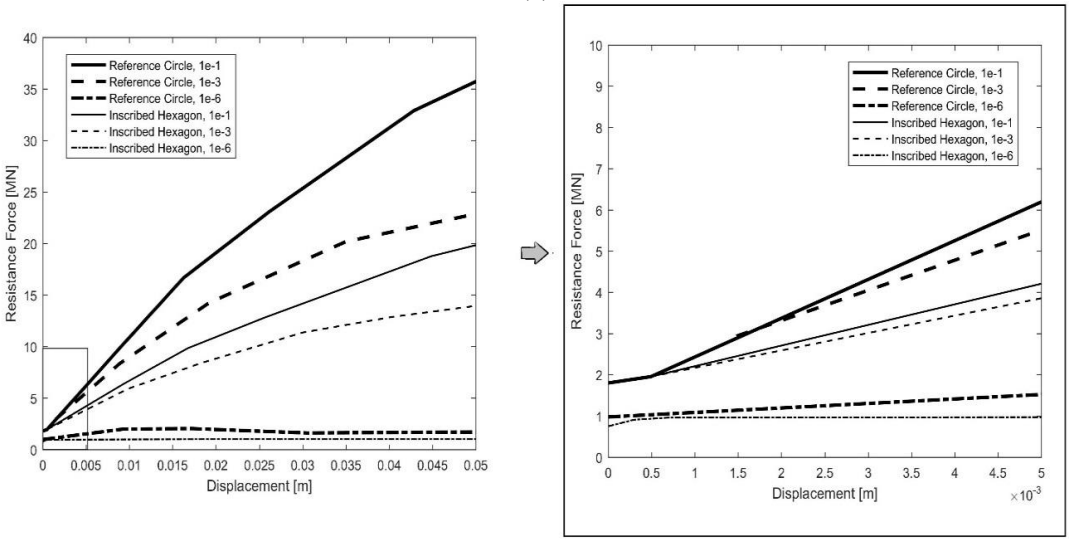

(c)

Fig. 19 Suction pressure for (a) inscribed pentagon, (b) peripheral pentagon, (c) inscribed hexagon and (d) peripheral hexagon

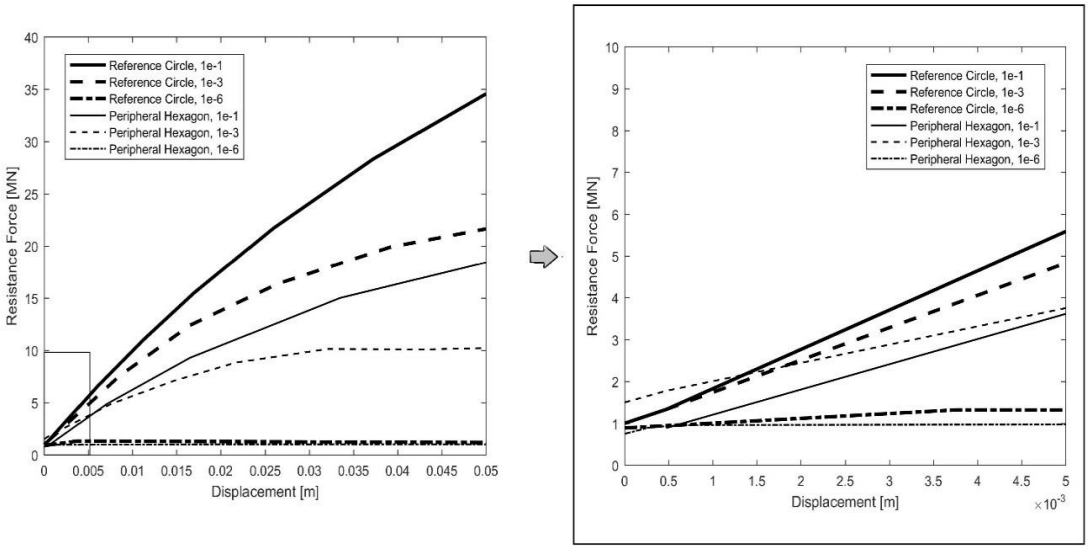

(d)

Fig. 19 Continued

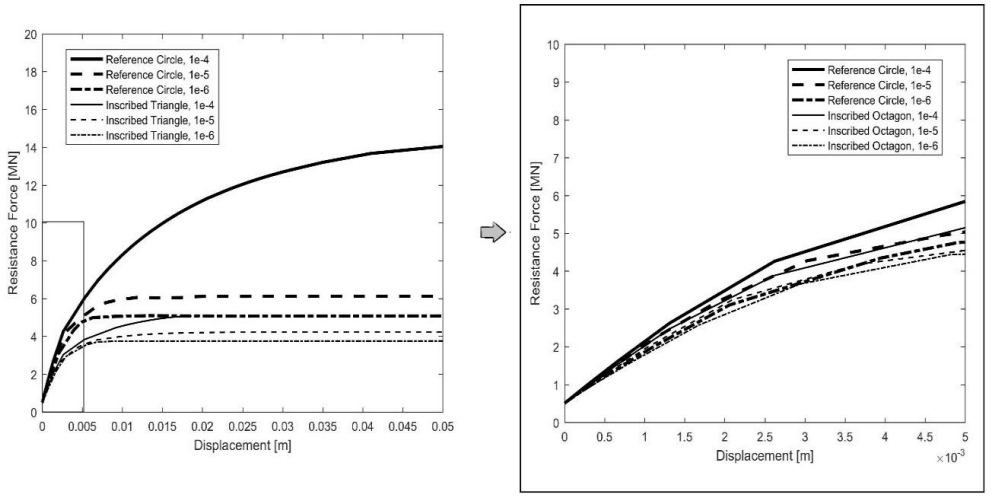

(a)

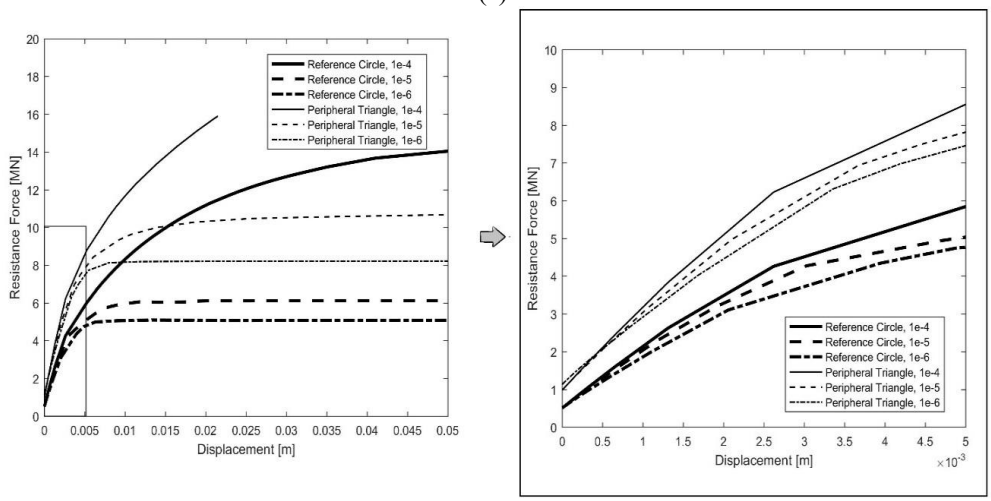

(b)

Fig. 20 Total resistance force for (a) inscribed triangle, (b) peripheral triangle, (c) inscribed octagon and (d) peripheral octagon

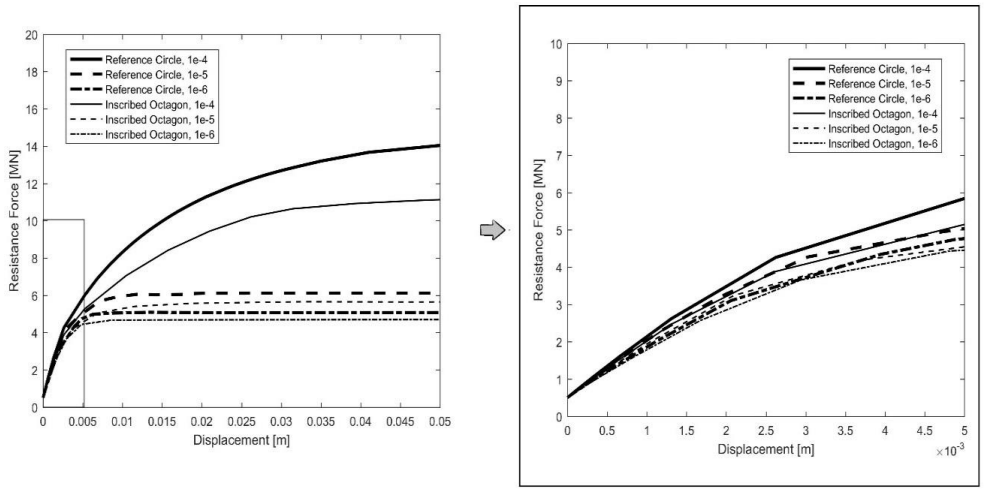

(c)

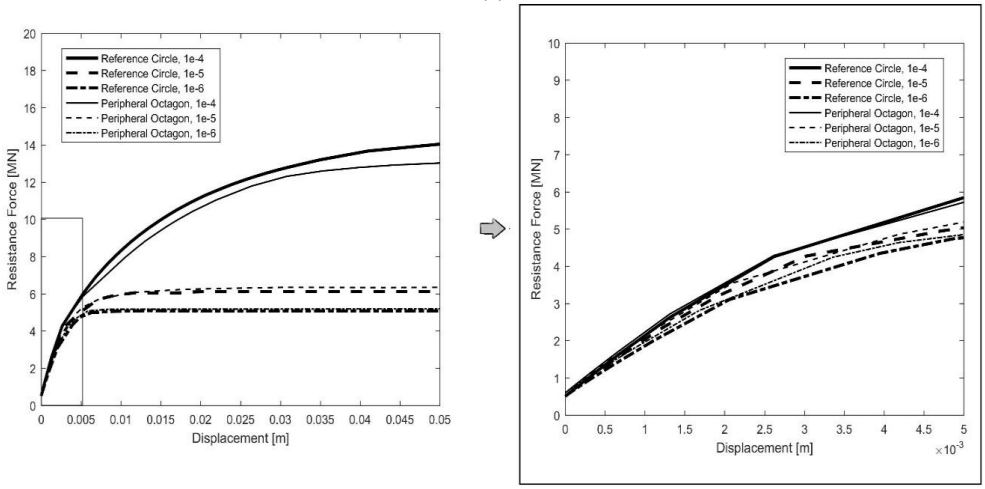

(d)

Fig. 20 Continued

resistance. In low velocities, drained behavior for the soil was governed and friction forces played a significant role in determining bucket resistance. Although the suction pressure for cylindrical geometry was higher than that of other geometries, the total resistance for some geometries was higher or lower than the reference one. That was expected since depending on the geometry, the contact area and the weight are higher or lower than the cylindrical one. By eliminating this contradiction through the division of resistance to the bucket weight, the results confirmed that the cylindrical geometry is the optimum geometry for designing suction caissons.

References

Achmus, M. and Thieken, K. (2014), "Numerical simulation of the tensile resistance of suction buckets in sand", *Proceedings of the 24th International Ocean and Polar Engineering Conference*, International Society of Offshore and Polar Engineers.

Ahlinhan, M.F., Houehanou, E.C., Koube, B.M. and Sungur, N. (2020), "3D Finite element analyses of suction caisson foundations for offshore wind turbines in drained sand", *Int. J. Geotech. Eng,*. **14**, 110-127, https://doi.org/10.1080/19386362.2019.1617500.

Ahmed, S.S. and Hawlader, B. (2014), "Finite element modeling of inclined load capacity of suction caisson in sand with Abaqus/Explicit", *Proceedings of the 24th International Ocean and Polar Engineering Conference*, Busan, Korea, June.

Alavi, A.H., Gandomi, A.H., Mousavi, M. and Mollahasani, A. (2010), "High-precision modeling of uplift capacity of suction caissons using a hybrid computational method", *Geomech. Eng.*, **2**(4), 253-280. https://doi.org/10.12989/gae.2010.2.4.253.

Bagheri, P. and Kim, J.M. (2019), "Evaluation of cyclic and monotonic loading behavior of bucket foundations used for offshore wind turbines", *Appl. Ocean Res*., **91**, 101865, https://doi.org/10.1016/j.apor.2019.101865.

Breton, S.P. and Moe, G. (2009), "Status, plans and technologies for offshore wind turbines in Europe and North America", Renew Energ., **34**, 646-654. https://doi.org/10.1016/j.renene.2008.05.040.

Bye, A., Erbrich, C., Rognlien, B. and Tjelta, T, (1995), "Geotechnical design of bucket foundations", *Proceedings of the Offshore Technology Conference*, Offshore Technology Conference.

Cao, J., Phillips, R., Popescu, R., Audibert, J.M.E. and Al-Khafaji, Z. (2002), "Numerical analysis of the behavior of suction

caissons in clay", *Proceedings of the 12th international offshore and polar engineering conference*. Kitakyushu, Japan.

Chong, S.H., Shin, H.S. and Cho, G.C.H. (2019), "Numerical analysis of offshore monopile during repetitive lateral loading", *Geomech. Eng.*, **19**(1), 79-91. https://doi.org/10.12989/gae.2019.19.1.079.

Cotter, O. (2009) "The installation of suction caisson foundations for offshore renewable energy structures". PhD Thesis, University of Oxford Magdalen College.

Ding, H., Hu, R., Zhang, P. and Le, C. (2020), "Load bearing behaviors of composite bucket foundations for offshore wind turbines on layered soil under combined loading", *Ocean Eng*., **198**, 106997. https://doi.org/10.1016/j.oceaneng.2020.106997.

Faizi, K., Faramarzi, A., Dirar, S. and Chapman, D, (2019), "Investigating the monotonic behaviour of hybrid tripod suction bucket foundations for offshore wind towers in sand", *Appl. Ocean Res.*, **89**, 176-187. https://doi.org/10.1016/j.apor.2019.05.018.

Fattah, M.Y., Al-Mosawi, M.J. and Al-Zayadi, A.O. (2013), "Time dependent behavior of piled raft foundation in clayey soil", *Geomech. Eng*., **5**(1), 17-36. https://doi.org/10.12989/gae.2013.5.1.017.

Gonzalez, J.Z. (2017), "Suction Bucket lid plate design and welding", Master Thesis, Aalborg University, Denmark.

Hendriyawan, M., Primananda, M.A., Puspita, A.D., Guo, C.H,, Hamdhan, I.N., Tahir, M.M., Pham, B.D., Muazu, M.A. and Khorami, M. (2019), "Simplification analysis of suction pile using two dimensions finite element modeling", *Geomech. Eng.*, **17**(4), 317-322. https://doi.org/10.12989/gae.2019.17.4.317.

Houlsby, G.T., Kelly, R.B. and Byrne, B.W. (2005), "The tensile capacity of suction caissons in sand under rapid loading", *Proceedings of the international symposium on fronteirs in offshore geotechnics*, 405-410. Perth (WA, Australia).

Ibsen, L.B., Hanson, M., Hjort, T. and Thaarup, M. (2009), "MC-parameter calibration of baskarp sand no. 15", Tech. rep. Department of Civil Engineering, Aalborg University, DCE Technical Reports; No 62.

Ibsen, L.B., Liingaard, M. and Nielsen, S.A. (2005), *Bucket Foundation, a status*. Copenhagen, Denmark: Copenhagen offshore wind.

Iskander, M., El-Gharbawy, S. and Olson, R. (2002), "Performance of suction caissons in sand and clay" *Can. Geotech. J.*, **39**, 576-584, https://doi.org/10.1139/t02-030.

Jin, Z.H., Yin, Z.Y., Kotronis, P. and Li, Z.H. (2019), "Advanced numerical modelling of caisson foundations in sand to investigate the failure envelope in the H-M-V space", *Ocean Eng*., **190**, 106394. https://doi.org/10.1016/j.oceaneng.2019.106394.

Kim, Y.S. and Choi, J. (2017), "Nonlinear numerical analyses of a pile-soil system under sinusoidal bedrock loadings verifying centrifuge model test", *Geomech. Eng.*, **12**(2), 239-255. https://doi.org/10.12989/gae.2017.12.2.239.

Lai, F., Liu, S., Deng, Y., Sun, Y., Wu, K. and Liu, H, (2020), "Numerical investigations of the installation process of giant deep-buried circular open caissons in undrained clay", *Comput. Geotech*., , **118**, 103322. https://doi.org/10.1016/j.compgeo.2019.103322.

Larsen, K.A. (2008), "Static behaviour of bucket foundations", Ph.D. thesis, Aalborg University, Denmark.

Latini, C. and Zania, V. (2019), "Vertical dynamic impedance of suction caissons", *Soils Found*, **59**, 1113-1127, https://doi.org/10.1016/j.sandf.2018.09.013.

Ma, P., Liu, R., Lian, J. and Zhu, B. (2019), "An investigation into the lateral loading response of shallow bucket foundations for offshore wind turbines through centrifuge modeling in sand", *Appl. Ocean Res*., **87**, 192-203. https://doi.org/10.1016/j.apor.2019.03.021.

Musial, W. and Ram, B. (2010), "Large-scale offshore wind power in the United States – assessment of opportunities and barriers", National Renewable Energy Laboratory, [TP-500-40745].

Nielsen, S.D. (2019), "Finite element modeling of the tensile capacity of suction caissons in cohesionless soil", *Appl. Ocen Res.*, **90**, 101866. https://doi.org/10.1016/j.apor.2019.101866.

Oh, K.Y., Nam, W., Ryn, M.S., Kim, J.Y. and Epureanu, B.I. (2018), "A review of foundations of offshore wind energy convertors: Current status and future perspectives", *Renew. Sust. Energ*. **88**, 16-36. https://doi.org/10.1016/j.rser.2018.02.005.

Rao, S.N., Ravi, R. and Prasad, B.S. (1997), "Pullout behavior of suction anchors in soft marine clays", *Mar. Georesour. Geotec*., **15**, 95-114. https://doi.org/10.1080/10641199709379939.

Samaniego, E., Anitescu, C., Goswami, S., Nguyen-Thanh, H., Guo, H., Hamdia, K., Zhuang, X. and Rabczuk, T. (2020), "An energy approach to the solution of partial differential equations in computational mechanics via machine learning: concepts, implementation and applications", *Comput. Method. Appl. Mech. Engrg.*, **362**, 112790. https://doi.org/10.1016/j.cma.2019.112790.

Schløer, S., Castillo, L.G., Fejerskoy, M., Stroescu, E. and Bredmose, H. (2016), "A model for quick load analysis for monopile-type offshore wind turbine substructures", *J. Phys. Conf. Ser.*, **753**, 092008. https://doi.org/10.1088/1742-6596/753/9/092008.

Schwägerl, C. (2016), Europe's offshore wind industry booming as costs fall, https://www.theguardian.com/environment/2016/oct/20.

Senders, M. (2008), "Suction caissons in sand as tripod foundations for offshore wind turbines", Ph.D. thesis, The University of Western Australia, Australia.

Skau, K.S., Jostad, P.J., Eiksund, G. and Sturm, H. (2019), "Modelling of soil-structure-interaction for flexible caissons for offshore wind turbines", *Ocean Eng.*, **171**, 273-285, https://doi.org/10.1016/j.oceaneng.2018.10.035.

Skempton, A.W. (1961), "Effective stress in soils, concrete and rocks", *Pore. Press. Suct. Soils*, 4-16, https://doi.org/10.1680/sposm.02050.0014.

Sørensen, E.S. (2016), "Numerical simulation of non-linear phenomena in geotechnical engineering", Aalborg Universitetsforlag.

Sørensen, E.S., Clausen, J. and Damkilde, L. (2017), "Comparison of numerical formulations for the modeling of tensile loaded suction buckets", *Comput. Geotech.*, **83**, 198-208. https://doi.org/10.1016/j.compgeo.2016.10.026.

Thieken, K., Achmus, M, and Schröder, C. (2014), "On the behavior of suction buckets in sand under tensile loads", *Comput. Geotech*, **60**, 88-100. https://doi.org/10.1016/j.compgeo.2014.04.004.

Vaitkunaite, E., Ibsen, L.B. and Nielsen, B.N. (2014), "New medium-scale laboratory testing of a bucket foundation capacity in sand", *Proceedings of the 24th, Int J Off Shore Polar*., Busan, South Korea.

Vaitkunaite, E., Nielsen, B.N. and Ibsen, L.B. (2016), "Bucket foundation response under various displacement rates", *Int. J. Offshore Polar Eng.*, **26**, 116-124. https://doi.org/10.17736/ijope.2016.jcr47.

Villalobos, F.A. (2006), "Model testing of foundations for offshore wind turbines", Ph.D. thesis, Oxford University, England.

Wriggers, P. and Laursen, T.A. (2006), *Computational contact mechanics* (Springer).

Zhu, B., Kong, D.Q., Tong, J.G., Kong, L.G. and Chen, R.P. (2011), "Model tests on penetration and pullout of suction caissons in silt", *J. Geotech. Eng*., **33**(7), 1045-1053 [in Chinese].

Zienkiewicz, O.C. and Shiomi, T. (1984), "Dynamic behavior of saturated porous media; the generalized Biot formulation and its numerical solution", *Int. J. Numer Anal. Meth. Geomech*., **8**, 71-96. https://doi.org/10.1002/nag.1610080106.

IC